The Astrophysical Journal, 603:L117–L120, 2004 March 10

A CORONAL THICK-TARGET INTERPRETATION OF TWO HARD X-RAY LOOP EVENTS

Astrid M. Veronig[1]
Institute for Geophysics, Astrophysics, and Meteorology, University of Graz, Universitätsplatz 5, A-8010 Graz, Austria
and
John C. Brown
Astronomy and Astrophysics Group, Department of Physics and Astronomy, University of Glasgow, Glasgow G12 8QQ, UK
Received 2003 September 29; accepted 2004 January 27; published 2004 February 20

ABSTRACT

We report a new class of solar flare hard X-ray (HXR) sources in which the emission is mainly in a coronal loop so dense as to be collisionally thick at electron energies up to $\gtrsim$50 keV. In most of the events previously reported, most of the emission is at the dense loop footpoints, although sometimes with a faint high-altitude component. HXR *RHESSI* data on loop dimensions and nonthermal electron parameters and *GOES* soft X-ray data on hot loop plasma parameters are used to model coronal thick-target physics for two "discovery" events (2002 April 14 [23:56 UT] and 2002 April 15 [23:05 UT]). We show that loop column densities N are consistent with (1) a nonthermal coronal thick-target interpretation of the HXR image and spectrum; (2) chromospheric evaporation by thermal conduction from the hot loop rather than by electron beam heating; and (3) the hot loop temperature being due to a balance of thick-target collisional heating and (mainly) conductive cooling.

Subject headings: Sun: flares — Sun: X-rays, gamma rays

On-line material: color figures

1. INTRODUCTION

Hard X-ray (HXR) flare imaging by the *Solar Maximum Mission* Hard X-ray Imaging Spectrometer (Hoyng et al. 1981; MacKinnon, Brown, & Hayward 1985) and by the *Yohkoh* Hard X-ray Telescope (HXT; Sakao 1994) found the HXR bremsstrahlung from accelerated electrons to be concentrated in loop footpoints, but with some faint HXR sources above the corresponding soft X-ray (SXR) loop (Masuda et al. 1994). The expected thick-target HXR height structure (Brown, Aschwanden, & Kontar 2002) confirms that "normal" HXR loops should be footpoint-dominated. In contrast, we report two flares with *RHESSI* HXRs coming mainly from the loop top with only weak footpoint emission. Both are gradual HXR events with very steep spectra and high coronal column densities.

2. OBSERVATIONS AND SCENARIO

RHESSI and *GOES* data on two flares (2002 April 14 [23:56 UT] and 2002 April 15 [23:05 UT]) near the northwest limb are studied (Table 1). *RHESSI* observes high-energy flare emission (3 keV–17 MeV) with high spectral and spatial resolution (Lin et al. 2002). During both events, the *RHESSI* thin attenuators (Smith et al. 2002) were in the field of view, limiting *RHESSI* data to $\gtrsim$6 keV.

Figure 1 (*top panel*) shows *RHESSI* light curves in four energy bands for the April 14 event, with 25–50 keV emission being detected for ~20 minutes. Figure 2 shows a *RHESSI* image sequence obtained with the CLEAN algorithm (Hurford et al. 2002). The 25–50 keV emission is concentrated near the loop top, although, during the impulsive rise (00:01–00:06 UT) and briefly during the late highest peak (00:10:22 UT), weak footpoint emission is detectable. Throughout, the soft 6–12 keV source is of comparable extent to the hard source (in contrast to normal events where HXRs are concentrated in a small footpoint volume). We conclude that the hot (SXR) plasma and the HXR-emitting electrons are close to cospatial in our events. Because the *RHESSI* spectral response drops sharply at energies $\simeq kT$, where T is the plasma temperature, T and the emission measure EM are best obtained from the *GOES* broadband response. *RHESSI* images are used to define $V = AL \simeq \pi Ad/2$, where A and d are the footpoint area and separation, respectively, and L is the loop length. The mean loop plasma density is then $n = (\mathrm{EM}/V)^{1/2}$ (for a filling factor of 1), and the loop leg column density $N = nL/2$. Figure 1 (*bottom panel*) shows the evolution of $N(t)$, $T(t)$ for this flare. As elaborated in § 3, these N-values are high enough to stop electrons $\lesssim$60 keV, which explains the absence of strong HXR footpoints.

RHESSI HXR spectra were derived in 1 keV bins during 4 s intervals using all front detectors except 2 and 7 (with lower spectral resolution and high threshold energies) and deconvolved with the full response matrix (Smith et al. 2002). We fitted these with various electron source models. Single isothermal fits are impossible since the spectra are (steep) power laws at high energies. The best fit was an isothermal plasma plus a power-law thick-target injection with index δ and power $P_{(25)}$ above 25 keV with an adjustable low-energy cutoff E_1. Figure 3 shows a sample together with the fit. There is no evidence of a "superhot" (Lin et al. 1981) component. The photon spectrum might also be fitted by a multithermal plasma, but polarized microwave emission (Nobeyama data) indicates nonthermal electrons. We thus propose a model with the power law from nonthermal thick-target emission (Brown 1971) in the dense loop, with isothermal plasma emission at lower energies. This leads to a self-consistent model in terms of energy balance and chromospheric evaporation, as well as of spectral fit. Figure 1 (*middle panel*) shows $P_{(25)}(t)$ and $\delta(t)$ for April 14. The inset is the locus of $P_{(25)}(t)$ versus $T(t)$ for the impulsive phase showing a distinct loop for the last peak (00:10–00:13 UT) when footpoints appear and when the spectrum is hardest ($\delta \simeq 6.7$).

Figure 4 shows the evolution of *RHESSI* fluxes, δ, $P_{(25)}$, N, and T for the April 15 flare. As for April 14, the HXR spectra are very steep. Figure 5 shows 6–12 and 25–50 keV *RHESSI* PIXON images indicating emission from two footpoints as well

[1] This work was partly performed during a research visit at NASA/Goddard Space Flight Center.

TABLE 1
EVENT CHARACTERISTICS

Date	Start Time (UT)	*GOES* Flare Class	Heliographic Position (deg)	A^a (10^{16} cm^2)	L^b (10^8 cm)	T_p^c (10^6 K)	EM_p^d (10^{49} cm^{-3})	N_p^e (10^{20} cm^{-2})	$P_{(25)p}^f$ (10^{28} ergs s^{-1})	δ_m^g
2002 Apr 14	23:56	M3.2	N20, W59	19.1	45.0	17.9	4.0	4.9	2.1	6.7
2002 Apr 15	23:05	M1.2	N20, W72	21.5	77.3	17.0	1.3	3.5	0.7	5.9

[a] Footpoint area.
[b] Loop length.
[c] Peak temperature.
[d] Peak emission measure.
[e] Peak column density.
[f] Peak total beam power in electrons ≥25 keV.
[g] Minimum electron spectral index.

as within the loop. Contrary to the April 14 event, during most of the impulsive phase, footpoint emission is seen.

3. THEORETICAL INTERPRETATION

3.1. *Coronal versus Footpoint Emission*

In normal HXR events, the coronal loop column density N is only capable of collisionally stopping electrons of fairly low energy, namely, $E_{\rm loop} = (3KN)^{1/2} \simeq 8.8N_{19}^{1/2}$ (keV) (Brown 1973), where $K = 2\pi e^4\Lambda$ (with e the electron charge and Λ the Coulomb logarithm) and $N_{19} = N/10^{19}$ (cm^{-2}). For the large peak values of N in Table 1, however, this gives $E_{\rm loop} \simeq 62$ keV (April 14) and $E_{\rm loop} \simeq 52$ keV (April 15). Even at the start of the April 14 impulsive HXR emission, $E_{\rm loop}$ is as high as 35 keV. Since only electrons of $E > E_{\rm loop}$ can reach the chromosphere, and since the spectra are so steep ($\delta \gtrsim 6.7$ in the April 14 event and $\delta \gtrsim 5.9$ in the April 15 event), we expect only very weak 25–50 keV footpoint emission. For a loop-top electron injection at a rate (per leg) $\mathcal{F}_0(E_0) = AE_0^{-\delta}$ (electrons s^{-1} per unit E_0), the thick-target emission at photon energy ϵ (for Kramers cross section $Q_0/\epsilon E$) from one loop half would be

$$I_{\rm tot}(\epsilon)\ (\text{photons s}^{-1}\ \text{per unit}\ \epsilon) = \frac{Q_0}{K\epsilon}\frac{A}{(\delta-1)(\delta-2)}\epsilon^{-\delta+2}, \quad (1)$$

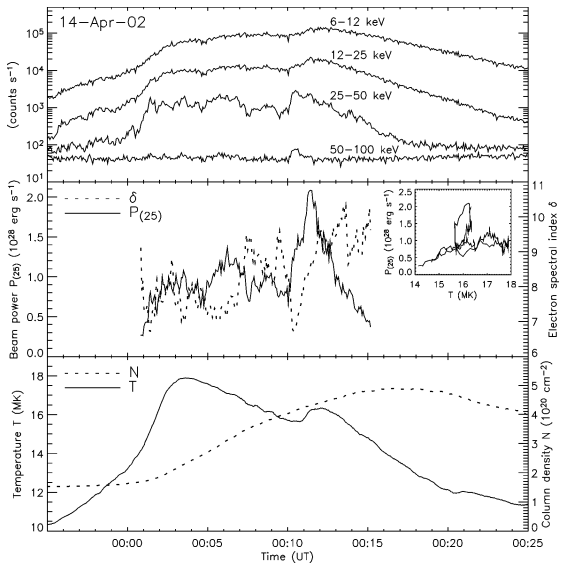

FIG. 1.—*Top panel: RHESSI* light curves for the April 14 event in four energy bands: 6–12, 12–25, 25–50, and 50–100 keV (scaled by factors of 5, 1, 4, and 1). *Middle panel:* Time history of electron spectral index δ and power in electrons ≥25 keV, $P_{(25)}$. *Bottom panel:* Time history of loop column density N and temperature T. The insert shows the locus of beam power $P_{(25)}(t)$ against temperature $T(t)$ for the impulsive phase.

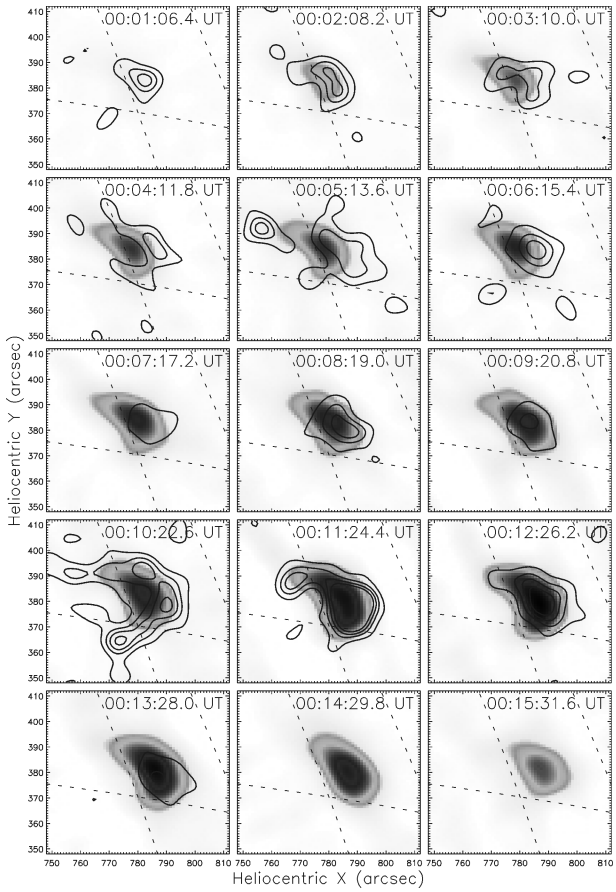

FIG. 2.—April 14 flare. Gray-scale images represent 6–12 keV *RHESSI* images reconstructed with CLEAN using grids 3–8 (except 7), giving an angular resolution of ~7″. The integration time of each image is 20.6 s, and the start times of consecutive images are separated by 61.8 s. The contours indicate the corresponding images at 25–50 keV (levels are 0.17, 0.3, 0.4, and 0.5). Images and contour levels are normalized to the respective maxima of the time series. [*See the electronic edition of the Journal for a color version of this figure.*]

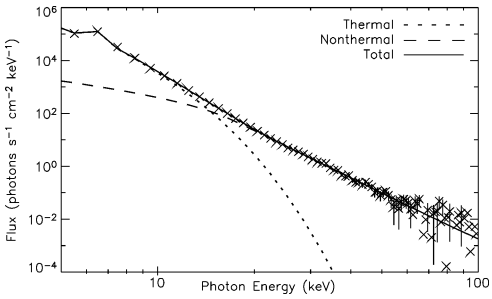

FIG. 3.—Sample spectrum of the April 14 flare, integrated over 4 s during the 25–50 keV maximum. The fit to the photon flux (*crosses*) is the bremsstrahlung from an isothermal plasma (*dotted curve*) and a single–power-law mean electron flux distribution with a low-energy cutoff (*dashed curve*). The solid curve represents the total fit. [*See the electronic edition of the Journal for a color version of this figure.*]

while the emission at ϵ by electrons of $E_0 > E_{\rm loop}$ reaching one footpoint would be

$$I_{\rm fp}(\epsilon) = \frac{Q_0}{K\epsilon}\frac{A}{2(\delta-1)}E_{\rm loop}^{-\delta+2}\int_0^{1/[1+(\epsilon/E_{\rm loop})^2]}\xi^{(\delta/2)-2}(1-\xi)^{-1/2}d\xi, \tag{2}$$

the ratio being

$$R = \frac{I_{\rm fp}(\epsilon)}{I_{\rm tot}(\epsilon)} = \frac{(\delta-2)}{2}B\left[\frac{1}{1+(\epsilon/E_{\rm loop})^2},\ \frac{\delta}{2}-1,\ \frac{1}{2}\right]\left(\frac{\epsilon}{E_{\rm loop}}\right)^{\delta-2}, \tag{3}$$

with B(a, b, c) the incomplete beta function. Here we neglected pitch angle changes (cf. Brown 1972) that give only a small correction to R. At $\epsilon = 25$ keV, this always gives $R \lesssim 0.2$, for $E_{\rm loop} \gtrsim 30$ keV and $\delta \gtrsim 6$.

3.2. *Origin of the High Coronal N- and T-Values*

A flare increase of N is attributed to radiatively unstable evaporation of chromospheric matter (Sweet 1969; Brown 1973) heated to $\gtrsim$60,000 K by electron beams or thermal conduction. Correcting Brown (1973) and modifying the treatment to closed loops, the coronal N for beam-driven evaporation is (see Kontar et al. 2003)

$$N_{\rm beam}\,({\rm cm}^{-2}) \simeq 8.2\times10^{19}\left[7.7\times10^{-12}B\left(\frac{\delta}{2},\frac{1}{3}\right)\times(\delta-2)\frac{P_{(25)}}{A}p\right]^{2/(\delta+2)}, \tag{4}$$

where $p \le 1$ corrects for finite loop-top pressure. This gives $N_{\rm beam} \lesssim 1.3\times10^{20}p^{1/4}$ cm^{-2} (April 14) and $N_{\rm beam} \lesssim 1.0\times10^{20}p^{1/4}$ cm^{-2} (April 15), much smaller than observed—i.e., much higher $P_{(25)}$ than observed is needed to create N by beam heating since most of the beam is stopped by the observed N.

Conductive evaporation near hydrostatic equilibrium at the event peak follows a Rosner, Tucker, & Vaiana (1978) scaling

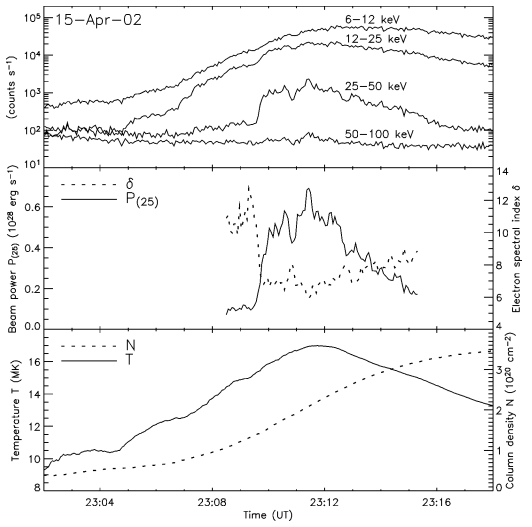

FIG. 4.—*RHESSI* light curves for the April 15 event in four energy bands (scaled by factors of 8, 4, 4, and 1). *Middle panel:* Time history of beam δ and $P_{(25)}$. *Bottom panel:* Time history of loop N and T.

law between loop pressure, T, and L (see Brown et al. 2000):

$${\rm EM}\,({\rm cm}^{-3}) = 7\times10^{47}\frac{A_{16}^2T_7^4}{L_9}, \tag{5}$$

but

$${\rm EM}\,({\rm cm}^{-3}) = n^2AL = 4\times10^{47}\frac{A_{16}N_{20}^2}{L_9}, \tag{6}$$

so that, equating to get the conductive N, we find

$$N_{\rm cond}\,({\rm cm}^{-2}) \simeq 1.4\times10^{20}T_7^2. \tag{7}$$

For the peak $T_7 = 1.8$ (April 14), $N_{\rm cond} \simeq 4.5\times10^{20}$ cm^{-2}, and for peak $T_7 = 1.7$ (April 15), $N_{\rm cond} \simeq 4.0\times10^{20}$ cm^{-2}, in good agreement with observations (see Table 1) suggesting that

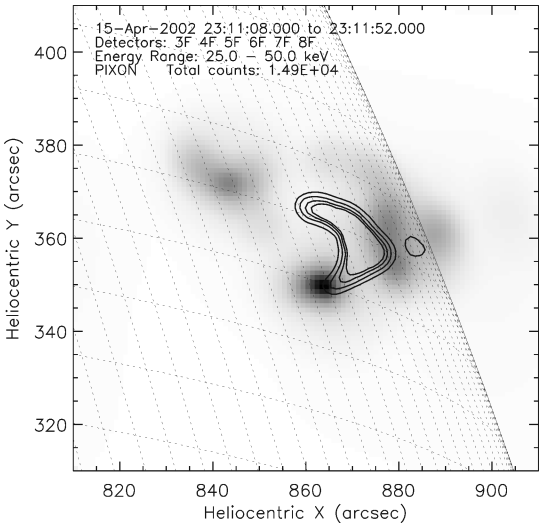

FIG. 5.—April 15 flare. The gray-scale image represents the 25–50 keV *RHESSI* image reconstructed with PIXON using grids 3–8 (integrated over 44 s during the 25–50 keV maximum). Contour levels at 0.2, 0.3, 0.4, and 0.5 of the peak flux indicate the corresponding 6–12 keV image. [*See the electronic edition of the Journal for a color version of this figure.*]

the high N results from conductive evaporation (see Aschwanden et al. 1997 concerning trapping).

The high N deposits most of the beam power in the loop top, so we check if the high loop T and $N_{\rm cond}$ could result from beam heating there. The flare energy budget is quite complex and time-dependent (Veronig et al. 2004). Here we simply estimate whether the beam power could create the peak T allowing for conductive and radiative cooling. This requires

$$4A\kappa_0 \frac{T^{7/2}}{L} + \mathrm{EM} f_{\rm rad}(T) = P_b, \tag{8}$$

where the first term is the conductive power out of both ends of the loop ($\kappa_0 = 10^{-6}$ ergs cm^{-1} s^{-1} K$^{-7/2}$). P_b is the total beam power deposited along the full loop length. In our two flares, most of P_b goes into the loop, but its value is very sensitive to the low-energy cutoff E_1, so we write $P_b = P_{(25)}\,(25/E_1)^{\delta-2}$. The radiative loss function $f_{\rm rad}(T)$ around 10^7 K is $f_{\rm rad} \simeq 6 \times 10^{-23} T_7^{-1/2}$ (ergs cm^3 s^{-1}), and equation (8) becomes

$$1.3 \frac{A_{16} T_7^{7/2}}{L_9} + 6\mathrm{EM}_{49} T_7^{-1/2} = \frac{P_{(25)}}{10^{26}} \left(\frac{25}{E_1}\right)^{\delta-2}. \tag{9}$$

Here we use equation (9) to find the E_1 needed to create the observed T. For April 14, we get $E_1 \simeq 31$ keV for mean $\delta \simeq 8$ and $E_1 \simeq 33$ keV for the hardest $\delta \simeq 6.7$. For April 15, we find $E_1 \simeq 27$ keV for mean $\delta \simeq 8$ and $E_1 \simeq 29$ keV for the hardest $\delta \simeq 5.9$. The best spectral fits for both give $E_1 \simeq 20$ keV, consistent with sufficient beam power to offset the observed losses.

4. DISCUSSION AND CONCLUSIONS

If R is the ratio of the emission at energy ϵ by electrons reaching the footpoints to the total emission (cf. eq. [3]), then $R/(1-R)$ gives the ratio of the footpoint emission to that within the loop. For footpoint area A and loop area $A_{\rm loop}$, the footpoint brightness per unit area compared with the loop is $b = (R/2A) / [(1-R)/A_{\rm loop}]$. For April 14, the ratio $A_{\rm loop}/(2A) \simeq L/(\pi A)^{1/2} \simeq 5.8$ (circular footpoints, semicircular loop). During the last peak when footpoint emission appears, $E_{\rm loop} \simeq 55$ keV, and the spectrum hardens from $\delta \simeq 9$ to $\delta \simeq 6.7$. For $\epsilon = 25$ keV, we predict b to increase from 0.02 to 0.16, which might explain the appearance of footpoints at this time, as the different sources become visible within the *RHESSI* dynamic range ($\lesssim 1:50$). However, the fact that the event shows different behavior in the ($P_{(25)}$, T)-locus then suggests that an additional physical process may be involved. For April 15, $A_{\rm loop}/(2A) \simeq 9.4$, and during the impulsive phase, we find $0.3 \lesssim b \lesssim 1.3$, consistent with the reconstructed images that, contrary to April 14, show footpoint emission throughout.

The Masuda "above the loop-top" sources found in impulsive flares during the impulsive peak were interpreted as evidence of magnetic reconnection above the SXR flaring loop. Our two events are different, showing HXR sources *within* the loop near the loop top; moreover, both are gradual flares. The different sensitivity, dynamic range, and spectral range of *RHESSI* and *Yohkoh*/HXT may explain why this class of events was not found by the HXT.

Brown & Emslie (1987) showed that spectral data cannot distinguish nonthermal and multithermal HXR models (cf. the Lin et al. superhot component), even with imaging spectroscopy, so recourse must be made to physical considerations. Here we have given a physically self-consistent nonthermal thick-target interpretation of the April 14 and 15 events.

We gratefully acknowledge the support of a PPARC rolling grant, of the Kanzelhöhe Summerschool (J. C. B.), and of the FWF grant P15344 (A. M. V.). A. M. V. thanks Brian Dennis, Richard Schwartz, Kim Tolbert, Linhui Sui, and Gordon Holman for their invaluable help with the *RHESSI* software and data interpretation.

REFERENCES

Aschwanden, M. J., Bynum, R. M., Kosugi, T., Hudson, H. S., & Schwartz, R. A. 1997, ApJ, 487, 936
Brown, J. C. 1971, Sol. Phys., 18, 489
———. 1972, Sol. Phys., 26, 441
———. 1973, Sol. Phys., 31, 143
Brown, J. C., Aschwanden, M. J., & Kontar, E. 2002, Sol. Phys., 210, 373
Brown, J. C., & Emslie, G. 1987, Sol. Phys., 110, 305
Brown, J. C., Krucker, S., Güdel, M., & Benz, A. O. 2000, A&A, 359, 1185
Hoyng, P., et al. 1981, ApJ, 246, L155
Hurford, G. J., et al. 2002, Sol. Phys., 210, 61
Kontar, E., et al. 2003, ApJ, 595, L123
Lin, R. B., Schwartz, R. A., Pelling, R. M., & Hurley, K. C. 1981, ApJ, 251, L109
Lin, R. P., et al. 2002, Sol. Phys., 210, 3
MacKinnon, A. L., Brown, J. C., & Hayward, J. 1985, Sol. Phys., 99, 231
Masuda, S., Kosugi, T., Hara, L., Tsuneta, S., & Ogawara, Y. 1994, Nature, 371, 497
Rosner, R., Tucker, W. H., & Vaiana, G. S. 1978, ApJ, 220, 643
Sakao, T. 1994, Ph.D. thesis, Univ. Tokyo
Smith, D. M., et al. 2002, Sol. Phys., 210, 33
Sweet, P. A. 1969, ARA&A, 7, 149
Veronig, A. M., Brown, J. C., Dennis, B. R., Schwartz, R. A., Sui, L., & Tolbert, A. K. 2004, ApJ, submitted